Mechanical properties and twin boundary drag in Fe–Pd ferromagnetic shape memory foils—experiments and *ab initio* modeling

To cite this article: I Claussen and S G Mayr 2011 *New J. Phys.* **13** 063034

New Journal of Physics
The open-access journal for physics

Mechanical properties and twin boundary drag in Fe–Pd ferromagnetic shape memory foils—experiments and *ab initio* modeling

I Claussen[1] **and S G Mayr**[2,3]

[1] I Physikalisches Institut, Georg-August-Universität Göttingen, Friedrich-Hund-Platz 1, D-37077 Göttingen, Germany
[2] Leibniz-Institut für Oberflächenmodifizierung eV, Translationszentrum für regenerative Medizin und Fakultät für Physik und Geowissenschaften, Universität Leipzig, Permoserstrasse 15, D-04318 Leipzig, Germany
E-mail: stefan.mayr@iom-leipzig.de

New Journal of Physics **13** (2011) 063034 (12pp)
Received 30 March 2011
Published 17 June 2011
Online at http://www.njp.org/
doi:10.1088/1367-2630/13/6/063034

Abstract. We report on vibrating reed measurements combined with density functional theory-based calculations to assess the elastic and damping properties of Fe–Pd ferromagnetic shape memory alloy splats. While the austenite–martensite phase transformation is generally accompanied by lattice softening, a severe modulus defect and elevated damping behavior are characteristic of the martensitic state. We interpret the latter in terms of twin boundary motion between pinning defects via partial 'twinning' dislocations. Energy dissipation is governed by twin boundary drag, primarily due to lattice imperfections, as concluded from the temperature dependence of damping and related activation enthalpies.

[3] Author to whom any correspondence should be addressed.

Contents

1. Introduction

Magnetic shape memory (MSM) alloys constitute an exciting new class of smart materials, which can yield magnetically switchable strains of several per cent at constant temperatures and frequencies up to some kilohertz. They are generally considered complementary to piezos or classical (thermal) shape memory materials—especially when requiring contact-less external control in an isothermal environment, e.g. in medical applications. In addition to Ni–Mn–Ga, where the MSM effect was initially discovered [1–3] and strains as high as 10% are achieved [4], Fe–Pd-based MSM alloys, which have been demonstrated to yield up to 5% strain in single crystals [5–7], are highly promising owing to their higher corrosion resistance, reduced brittleness and recently demonstrated biocompatibility [8]. Although macroscopic properties and processing of bulk Fe–Pd samples are rather well established, the latter are much less understood when miniaturized. In particular, phase formation and twin boundary mobility are severely affected by the presence of open surfaces, substrates, strain fields and lattice defects—which on the one hand reveal an additional complication, but also bear the potential for optimization and new applications [9]. In fact, as recently shown for the complementary Ni–Mn–Ga system, maximum strains are feasible not only in single crystals, but also in porous polycrystals (i.e. in the presence of sufficient surfaces to relieve constraints) [10]. This hints at the high potential of appropriately processed polycrystalline foils based, for example, on the melt spinning [11–14] or splat quenching [15] techniques to achieve the desired face-centered tetragonal (fct) martensitic phase by a rapid quench of the austenitic face-centered cubic (fcc) lattice. These foils present an economical alternative to freestanding single crystalline films that can be grown, for example, by molecular beam epitaxy [9] and subsequently have to be lifted off the substrate [16].

The MSM effect is based on a magnetic-field-induced reorientation of martensite variants, which is known to occur via twin boundary motion once the equivalent magnetic stresses overcome the twinning stress, σ_t [17]. For high enough magnetic fields the maximum attainable equivalent magnetic stresses are limited by the magnetic anisotropy, K_1, as it prevents rotation of the magnetic moments. That is, the maximum tolerable twinning stress is given by $\sigma_t < K_1/\epsilon_0$, where ϵ_0 denotes the maximum theoretical strain given solely by the lattice geometry of the martensite. On the microscopic scale, it is well established that reorientation of martensite

variants and the associated twinning stress are determined by nucleation and motion of twinning dislocations, while the detailed martensite structure in response to microstructural or external boundaries can be understood based on its adaptive nature to minimize elastic energy [18, 19]. In polycrystalline foils, nucleation of twinning dislocation is expected to preferentially occur from the open surface or grain boundary and also via dislocation loops at the variant interfaces—and has been treated extensively in the literature since the 1950s [20] with respect to required stress. The aim of this paper is to assess the second aspect of twin boundary mobility: the drag exerted on twinning dislocations in splat-quenched Fe–Pd MSM foils.

2. Experimental details

Samples were prepared from prealloyed ingots with nominal compositions $Fe_{70}Pd_{30}$ and $Fe_{71}Pd_{29}$, respectively, which were alloyed in the liquid phase by arc melting with an approximate accuracy of 0.01 atomic per cent. To ensure homogenization, the ingot was turned over and extensively melted six times. After transferring the material to a splat quencher, which was purged six times with Ar (purity 99.998%) to ensure well-defined experimental conditions, the ingots were melted inductively and rapidly solidified by splatting between two copper pistons [21]. The resultant foils have diameters between 20 and 30 mm and thicknesses of $\approx 50\,\mu$m and are stochiometrically isotropic within the resolution of state-of-the-art energy-dispersive x-ray spectroscopy (EDX); in the following they are referred to as *splats*. As the *as-prepared* splats reveal a rough surface and a rough rim at the outer radius, they were polished to obtain a homogeneous surface. In the course of rapid solidification, the alloy crystallizes in the fcc austenitic phase, finally yielding at room temperature fcc austenite or fct martensite for $Fe_{70}Pd_{30}$ and $Fe_{71}Pd_{29}$, respectively. Room temperature phases and martensitic transformation were verified by temperature-dependent x-ray diffraction (XRD) measurements using Cu-K_α radiation in a $\theta/2\theta$ geometry. As the tetragonality of the crystal unit cell increases, the fcc (200)-peak shifts to the fct (200) position, so that martensite start temperature ($M_s(Fe_{70}Pd_{30}) = 13 \pm 5\,^\circ$C, $M_s(Fe_{71}Pd_{29}) = 52 \pm 5\,^\circ$C) and martensite finish temperatures ($M_f(Fe_{70}Pd_{30}) = -9 \pm 5\,^\circ$C, $M_f(Fe_{71}Pd_{29}) = 30 \pm 5\,^\circ$C) can be determined. Within this context, it is interesting to note that despite reaching M_f, the tetragonal distortion increases further during cooling down by an additional ≈ 100 K, as reported previously [15]. Strips with a length of 25 mm and a width of 5 mm were cut from the splats to study their mechanical properties in a home-built vibrating reed experiment specially designed for measuring splats. Our setup allows for the cycling of sample temperatures between -70 and 200 °C, which was performed at very low heating rates to ensure thermal equilibrium at all times. On one side, the sample is rigidly clamped in a stainless steel mount, with a thermal expansion close to that of Fe–Pd to avoid loosening of the clamp during heating or cooling. The samples, which have a free length of ≈ 17 mm, form a capacitor with a gold electrode and are excited to vibrations by an alternating voltage modulated onto a bias voltage. The vibration of the sample is detected by the deflection of a laser beam, which is reflected from the sample onto a position-sensing detector. With a sufficiently long light path this setup—with a resulting curvature resolution of 30 km or better—allows for the detection of very small movements and avoids cross-talk between excitation and detection. For the investigation of temperature-dependent changes in elastic modulus and damping properties, the samples were first excited to vibrations with a frequency close to their resonance to obtain a maximum oscillation amplitude. From the subsequent free decay the exact eigenfrequency and damping Q^{-1} were determined.

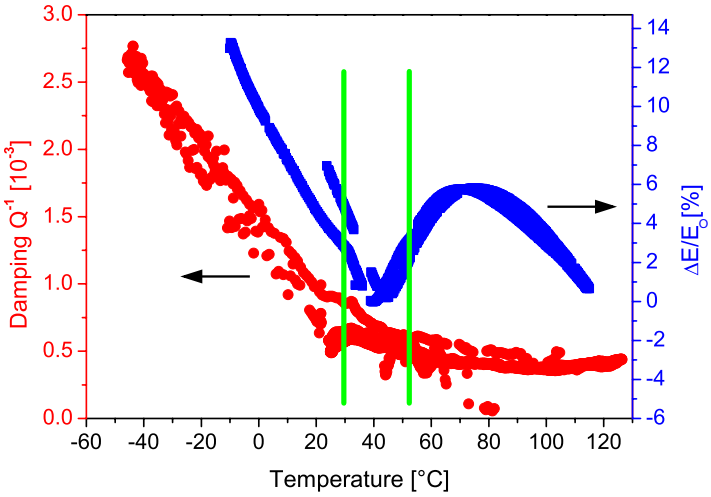

Figure 1. Relative changes in Young's modulus, $\Delta E/E_0$, and damping, Q^{-1}, during free oscillations of a $Fe_{71}Pd_{29}$ splat in a vibrating reed apparatus. The two vertical bars indicate the regions of martensite transition, as determined from XRD measurements (figure 2).

3. Experimental results

The vibrations of a bar that is clamped at one end belong to the standard problems of continuum mechanics, which are covered in many textbooks (e.g. [22]): the Young's modulus, E, can be obtained from the frequency f of the first mode of the free oscillation via

$$E = 12\left(\frac{2\pi}{1.875^2}\right)^2 \cdot \frac{L^4}{d^2}\,\rho\, f^2, \tag{1}$$

where L, d and $\rho = 8.9 \times 10^3\,\mathrm{kg\,m^{-3}}$ denote the sample length, thickness and density[4], respectively. In the following, two samples will be focused on: a room-temperature austenitic $Fe_{70}Pd_{30}$ splat with length $L = 16.7 \pm 0.5$ mm and thickness $d = 47 \pm 8\,\mu$m vibrating with a frequency $f = 76.7 \pm 0.1$ Hz, which yields an elastic modulus of $E = 72 \pm 10$ GPa. Accordingly, a martensitic $Fe_{71}Pd_{29}$ sample ($L = 16.8 \pm 0.5$ mm, $d = 59 \pm 6.5$ m and $f = 112.8 \pm 0.2$ Hz) reveals $E = 100 \pm 11$ GPa at room temperature. The evolution of Young's modulus E and damping Q^{-1} is studied as a function of temperature for both samples. As E varies strongly during austenite–martensite phase transformation, it is convenient to study the modulus defect $\Delta E/E_0$ as depicted in figure 1. To facilitate a comparison of samples with different compositions, which transform at different temperatures, the latter is normalized to the smallest value E_0 obtained at the end of the phase transition. In samples with a Pd content of 29%, the elastic modulus increases almost linearly with decreasing temperature at temperatures well above and below the phase transformation, respectively, as expected for metallic samples due to Debye–Grüneisen expansion (figure 1). During austenite–martensite phase transition, i.e. changing the temperature between M_S and M_F, $\Delta E/E_0$ yields a strong decrease, indicating a shear softening of the parent austenite phase. The steepest slope of $\Delta E/E_0$ occurs at

[4] The density was estimated from the molar masses of Fe and Pd and the volume of the unit cell of the austenite.

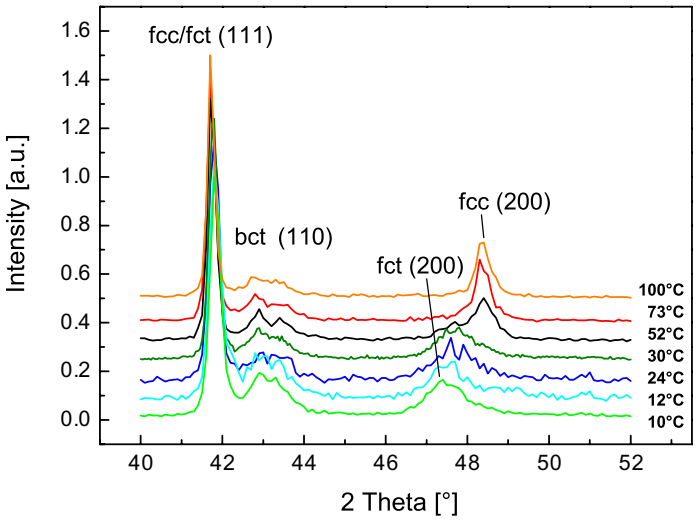

Figure 2. XRD measurement indicates a austenite–martensite transition in an $Fe_{71}Pd_{29}$ splat between 30 and 52 °C. Note that not all martensitic variants are present and minor amounts of bct martensite are detected at all temperatures.

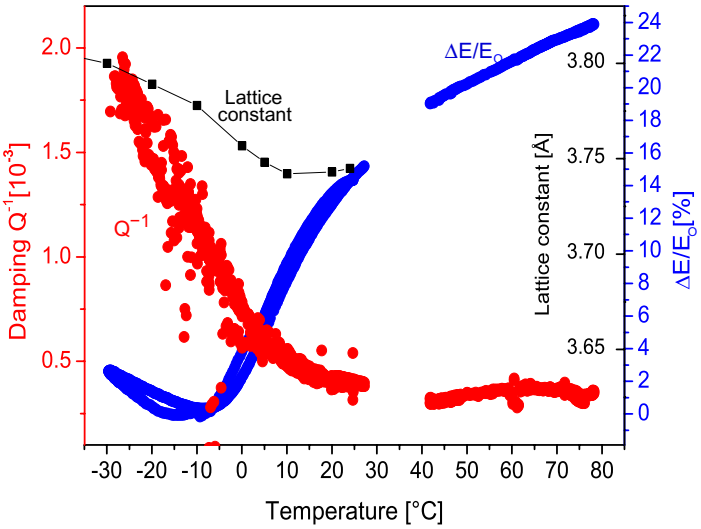

Figure 3. Relative Young's moduli, damping behavior and fcc/fct(200) lattice constants as a function of sample temperature for an *as-prepared* $Fe_{70}Pd_{30}$ splat.

the temperature for which the onset of tetragonal distortion has been determined by XRD (figure 2). However, as the severe drop in $\Delta E/E_0$ with decreasing temperature already occurs at significantly higher temperatures, this might indicate that $\Delta E/E_0$ is more sensitive to martensite transformation than x-ray measurements in detecting the presence of premartensite starting from temperatures just below ≈80 °C. Samples with a Pd content of 30% (figure 3) show a slightly different behavior: decrease of $\Delta E/E_0$ starts at temperatures well above the phase transition and is more distinct than that for $Fe_{71}Pd_{29}$; over the entire temperature range, $\Delta E/E_0$ changes by 24%. For both compositions, damping is almost constant at high temperatures and dramatically increases toward low temperatures within the fct martensitic phase. To make sure

that the increase in damping as seen in figures 1 and 3 was not caused by the experimental setup, e.g. the clamping of the sample, additional measurements were carried out with a piece of Si wafer, which is known to have very low intrinsic damping. The damping measured on the Si wafer is about one order of magnitude lower than the damping of the splats, and the typical increase of damping with decreasing temperature, as observed on all splats, cannot be seen for the Si wafer. Thus, the damping caused by the experimental setup can be separated from the damping of the splats, and it becomes clear that the increase of damping must be an intrinsic property of the splats.

4. Numerical methods

When quenched from the melt, $Fe_{70+\delta}Pd_{30-\delta}$ around the $|\delta| \lessapprox 2$ composition experimentally reveals a rather complex metastable phase diagram with a high-temperature austenite (fcc–γ) phase and two martensitic phases—a less distorted fct and a more distorted body-centered tetragonal (bct) phase, respectively [5, 32]—which can be considered to be connected by an idealized Bain path [33, 34]. Note that all involved phases reside in a disordered solid solution—the disorder, in fact, also constitutes the greatest challenge from a modeling point of view. Within the framework of density functional theory (DFT) [23], several approaches have been suggested in order to cope up with the challenges brought about by disorder—including the virtual crystal approximation (VCA), coherent potential approximation (CPA) and special quasi-random structures (SQS) [30]. As only the SQS approach allows one to include ionic relaxations, which are expected to be highly relevant experimentally because of the size difference of the atomic constituents in the present system, and to assess the mechanical response, we decided to stick to the latter in the following. In fact, previous DFT calculations employing a rigid lattice in the CPA indicate the presence of local minima of the ground state energy [34, 35], which seem to be strongly influenced by the absence of ionic relaxations. Within this context, we would like to emphasize that although we benefit from structurally relaxed SQS cells, on the other hand we pay the price of (i) requiring significantly more computational resources (demanding large-scale simulations on supercomputers) and (ii) lower flexibility in choosing the desired stochiometry. Both (i) and (ii) make it impossible for us to 'exactly' model $Fe_{70}Pd_{30}$ or $Fe_{71}Pd_{29}$. Because of the availability of reasonably sized SQS supercells [31] that have been evaluated with respect to mechanical properties, we decided to stick to a composition close by, namely $\delta = -1.25$, in the following to fulfill these requirements as a compromise.

DFT [23]-based total energy calculations were performed to study the structural and mechanical properties of the Fe–Pd martensitic phase from a theoretical point of view. We employed the projector-augmented wave (PAW) approach [24, 25] and generalized gradient approximation (GGA) of Perdew and Wang (PW91) [26] in connection with the spin interpolation formula of Vosko *et al* [27], as implemented in the Vienna *ab initio* simulation package (`vasp`) [28]. The cutoff of the plane wave basis set was chosen high enough (348.27 eV) to ensure reliable treatment of the $3d^74s^1$ Fe and $4d^95s^1$ Pd pseudopotentials supplied by `vasp` and determination of the stress tensor. Sampling of the Brillouin zone was optimized to obtain a convergence better than 0.5 meV atom^{-1}, which was reached by employing at least 1152 k-points $\times$ atoms with a Γ centered mesh for the SQS cells discussed above. In fact, a high accuracy is urgently required in order to correctly reproduce the narrow potential energy landscape expected within the martensitic phase [29]. Mechanical properties are determined by two independent standard methods: the first one includes following the energy changes as a

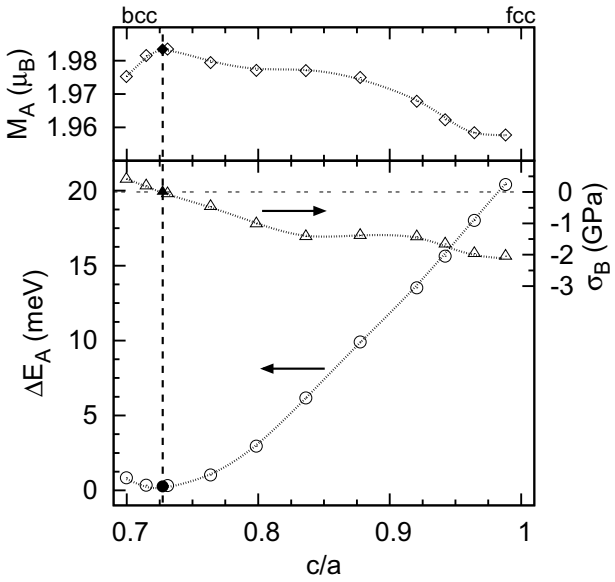

Figure 4. DFT calculations on the electronic and ionic ground states of a $Fe_{68.75}Pd_{31.25}$ SQS supercell at variable biaxial strains in the a directions and zero stress maintained in the c-direction of the tetragonal simulation cell. The ground state energy per atom, ΔE_A, as a function of tetragonal distortion, c/a, shows a global minimum for a bct structure at $c/a = 0.727$ (as marked with filled symbols in the plot). As expected, the biaxial stresses, σ_B, vanish at the location of the minimum, while the bcc and fcc lattices clearly become unstable. The magnetic moment per atom, M_A, shows a distinct maximum for the equilibrium structure.

function of small deformations into elastically independent directions followed by a successive derivation of the resulting curve, while the second one is based on direct calculation of stresses in response to small strains. In this context, we would like to note that while the latter is generally considered less reliable with respect to errors, similar accuracies could be achieved within this paper due to a sufficiently high energy cutoff.

5. Ground state and mechanical properties of $Fe_{68.75}Pd_{31.25}$

To identify the ground state crystal structure, we decided not to follow strictly the Bain path, as it is generally accepted that it does not strictly give the transformation path in martensites. Instead, we allowed relaxations of the atomic coordinates and the box dimension in the z direction for a series of fixed biaxial strains. This approach systematically led to lower ground state energies and a differently shaped potential energy landscape than the strict Bain transformation path at constant volume and/or with rigid atomic positions. The latter have to be considered to be highly idealized, while a biaxial transformation approach with zero stress maintained in the z-direction of the open surfaces most realistically mimics our experimental thin foil geometry.

In figure 4, the resulting ground state energies per atom, ΔE_A—relative to the lowest energy level—are plotted as a function of tetragonal distortion, c/a, of the relaxed SQS $Fe_{68.75}Pd_{31.25}$ simulation cell. Similar to a CPA approach on a slightly different stoichiometry

Table 1. Elastic moduli, C_{ij}, in units of GPa, as determined from DFT calculations for $Fe_{68.75}Pd_{31.25}$ SQS supercells at the energy minimum. Row (i) corresponds to the minimum in figure 4, while row (ii) was generated by allowing for orthorhombic distortion during further relaxation of (i). As, however, C_{ij} for (ii) revealed only negligible deviations from tetragonal symmetry, only the corresponding components are given.

	C_{11}	C_{12}	C_{13}	C_{33}	C_{44}	C_{66}
(i)	268	81.6	167	175	98.7	12.9
(ii)	270	81.8	166	172	98.8	12.8

of Fe–Pd with fixed atomic positions and constant volume [34], the resulting ground state energy landscape in this paper proves to be very shallow, with typical barriers as low as some meV, while the detailed shape reveals different signatures: clearly, a global energy minimum is discernible at $c/a = 0.727$, which is accompanied by vanishing biaxial stresses, σ_B, as expected. The six independent components of the tensor of elasticity of the minimum energy tetragonal SQS cell were determined, as described in section 4 and given in table 1 (i). In addition to the tetragonal SQS cell, a second orthorhombic cell (ii) was considered, which was prepared by starting from (i) and then allowing for further relaxation due to additional orthorhombic cell distortions. Due to the similarity of (i) and (ii), however, we conclude that orthorhombic distortions are negligible to the current problem—which is also interesting to note in relation to the currently employed SQS approach.

While table 1 refers to a perfect $Fe_{68.75}Pd_{31.25}$ single crystal, applications and experiments will often also employ polycrystalline samples. It is therefore highly desirable to also give estimates for the corresponding polycrystal elastic constants[5]. Generally, the problem of giving bounds for polycrystal elastic constants from the corresponding single-crystal properties has attracted much interest from the beginning of metallurgy [36, 37] and is still a topic of current research (e.g. [38]). At present, we employ the self-consistent approach, originally proposed by Kröner [39] for cubic crystals, approximately to our tetragonally distorted system by (a) averaging the tensor of elasticity over all spatial directions and (b) then applying the Kröner algorithm; the results are shown in table 2. With respect to the robustness of the values given in table 2, we would like to note that we observed only a minor deviation when choosing a different location on the potential energy landscape of figure 4 by applying a fixed c/a constraint (which, of course, is straightforward for the bulk modulus).

6. Estimation of twin boundary drag

We proceed by relating the experimental findings of section 3 to the results of our simulation work in section 5. We start by assuming that the elastic constants in table 2 give a good approximation for a hypothetical defect-free polycrystalline martensitic $Fe_{71}Pd_{29}$ splat, which resides in a bct/fct mixture at room temperature and—in accordance with [5]—transforms to the

[5] Despite a columnar microstructure the splats do not reveal any crystallographic texture, as inferred from pole figure measurements; see [48].

Table 2. Kröner's self-consistent estimates of the elastic constants (bulk modulus Ξ, Young's modulus E, Poisson ratio ν and shear modulus G) of $Fe_{68.75}Pd_{31.25}$ polycrystals.

	Ξ (GPa)	E (GPa)	ν	G
(i)	171	163	0.341	60.9
(ii)	171	164	0.340	61.2

bct phase in the low-temperature regime[6]. Discrepancies between DFT predictions ($E(0\,\mathrm{K}) \approx 171\,\mathrm{GPa}$) and experiments ($E(263\,\mathrm{K}) \approx 113.5\,\mathrm{GPa}$) will mostly be based on the presence of lattice defects in the experimental samples—besides minor[7] Debye–Grüneisen/thermal-expansion-related contributions. It is well established that in the martensitic state, defects are most prominently twins, while a reduction in elastic constants is generally attributed to twin boundary motion mediated by partial dislocation (often called 'twinning dislocation') glide. While in perfect infinite Fe–Pd single crystals, resistance against twin boundary motion is generally attributed to homogeneous nucleation of twinning dislocations [18, 19], things are expected to be different in splat-quenched polycrystals. In the course of rapid quenching, we expect the presence of large quantities of dislocations, as experimentally corroborated by a very fine lamellar martensite 'variant' microstructure. It is most reasonable to assume that under these conditions, twin boundary motion is not limited by nucleation, but rather by pinning of twin boundaries. In fact, with expected twinning stresses in perfect single-crystalline Fe–Pd in the range of some MPa [40], the rather high apparent elastic moduli determined by vibrating reed in our splats hint at a limited mobility of the twin boundaries by pinning of twinning dislocation at lattice defects. In the presence of an external oscillating shear stress (such as in our vibrating reed apparatus), it is therefore most reasonable to assume that twinning dislocations perform a 'vibrating string model' type of motion [22, 41], thus reducing the elastic moduli in comparison to the DFT calculations and dissipating energy via drag on twinning dislocations.

In the following, we develop this picture further to estimate the drag on twinning dislocations, which we term 'twin boundary drag', B, below. We start our analysis with the predictions of the Granato and Lücke vibrating string model [41] for the modulus defect and energy dissipation (equations (3.11) and (3.12) of [41], respectively), which—in their low-frequency limit—can be combined to yield

$$B \approx \frac{G_{\mathrm{DFT}}^2\, b^2\, Q^{-1}}{l^2\, f\, (1-\nu_{\mathrm{DFT}})\, (G_{\mathrm{DFT}} - G)}, \tag{2}$$

where b, Q^{-1}, f, l, ν_{DFT}, G and G_{DFT} denote Burger's vector of a twinning dislocation, vibrating reed damping loss, vibrating reed frequency, distance between pinning defects, DFT-based estimation of the Poisson ratio, measured shear modulus and DFT prediction, respectively. To quantify the typical magnitudes of B in martensitic $Fe_{71}Pd_{29}$ splats, we first approximate the typical distance between pinning defects with the splat grain size [15] $l \approx 175\,\mathrm{nm}$. It is also reasonable to assume that the DFT-determined Poisson ratio is also a good estimate for experiments, which yields $G(T = 263\,\mathrm{K}) \approx 40.2\,\mathrm{GPa}$. With $Q^{-1}(T = 263\,\mathrm{K}) \approx 1.7 \times 10^{-3}$,

[6] An extensive review of the phase formation and transitions of splats can be found in [48].

[7] In particular due to the Invar properties of this alloy, thermal expansion is moderate [47].

$f \approx 117$ Hz and $b \approx 0.79$ Å (calculated with the methods given in [42] employing the values $a \approx 4.17$ Å and $c \approx 3.03$ Å as determined from the minimum of the DFT calculations (figure 4) and assuming {011} twinning planes), we obtain for the magnitude of $B(T = 263\,\mathrm{K}) \approx 0.80$ Pa s, which constitutes a rather large value when compared with typical drag coefficients of moving full dislocations in metals with dominant electronic or phononic contributions [20]. In fact, due to the preparation technique of our splats and the nature of the Fe–Pd alloy, we expect a significant impact of structural obstacles (atomic disorder, defect-, variant- and microstructure, as well as related stress fields) on dislocation mobility—ranging from increased drag to full pinning. This view is corroborated by a severe increase of damping—and drag—with reduced temperature, which hints at the presence of thermally assisted dislocation mobility at obstacles: while at severe lattice distortions twinning dislocations get fully pinned, they can overcome minor obstacles by thermal activation, thus leading to a temperature-dependent viscous behavior—just like in the Eyring theory for viscous flow [43]. Based on this picture, the corresponding activation enthalpy is readily calculated by performing an Arrhenius fit of $B(T)$ deep in the martensitic phase, yielding $\Delta H = (0.17 \pm 0.03)$ eV—which is perfectly reasonable for the suggested explanation. From a technical point of view, our quantitative analysis thus indicates the potential use of Fe–Pd splats in low-frequency/quasistatic MSM applications, or—vice versa—magnetically controllable damping elements.

7. Mechanical properties around the martensite transition

Until now, our discussion has only focused on the mechanical properties in the pure martensitic state. On the other hand, strong signatures are evident across the austenite–martensite phase transition—particularly in the elastic modulus. Much understanding in this context has been obtained from numerous investigations on 'classical'-shape memory alloy, as discussed in e.g. [44]. Starting from high temperature, the continuously dropping Young's modulus, E, in $Fe_{70}Pd_{30}$ starting at temperatures well above transformation can be understood as the softening of certain phonon modes ('pre-martensite') [31] prior to martensite transformation [45]. Interestingly, that kind of softening is not observed in $Fe_{71}Pd_{29}$, namely the macroscopic instability necessary for phase transition according to Owen [46] seems to be absent. As the martensite transition in $Fe_{71}Pd_{29}$ is located close to the triple point between fcc, fct and bct phases [5], we speculate that the concurrent presence of all three phases is responsible for this scenario. In fact, as martensite transition to the bct phase is generally considered irreversible [5], it is most reasonable that those portions of the sample already revealing bct phase greatly lack soft modes. Coherent with the surrounding fcc and fct phases, these bct nuclei will certainly have a macroscopic hardening effect and prevent overall softening due to premartensite formation.

The damping properties of splats with Pd content of 29 and 30% are very similar and do not seem to be connected to the changes in elastic modulus discussed above. We interpret this as strong corrobation that, in fact, twin boundary motion in fct and bct martensites is the underlying physics—not the phase transition. As can be seen from figures 1 and 3, damping is almost constant at high temperatures and dramatically increases during phase transition. This increase continues to low temperatures—in contrast to phase-transition-related damping peaks [44]. We surmise that the absence of the latter is related to a suppression of the mobility of martensite–austenite interfaces by the foil microstructure. In contrast to our measurements, Nakajima *et al* [13] reported on melt-spun ribbons with a Pd content of 29.6%, which show several maxima, which are attributed to the phase transition. However, at the temperatures

where these maxima occur, no distinct changes in the elastic modulus or other sample properties are observed that would indicate the phase transition. Moreover, the damping measured by Nakajima *et al* is around $Q^{-1} = 3 \times 10^{-3}$ and thus about five times as large as the damping observed in the present experiments. Assuming that melt-spun ribbons and splats, which were both rapidly quenched from the melt, have similar intrinsic damping properties, one might suspect that the damping measured by Nakajima *et al* not only displays intrinsic damping of melt-spun ribbons, but also includes other effects.

8. Conclusions

All in all, we have employed a combined experimental–simulational approach to assess the physical foundations of the mechanical response of rapidly solidified Fe–Pd MSM foils in the martensitic phase. In our picture, the occurrence of a shear modulus defect and damping is the result of a defect-limited motion of partial 'twinning' dislocation between pinning sites, while drag is established by thermal activation to overcome minor obstacles. Systematic analysis allows us to estimate the corresponding twin boundary drag in the range of 0.80 Pa s. Elastic moduli reveal a strong fingerprint of austenite–martensite transition, which can be observed as a precursor phenomenon of the martensitic transformation in samples with a Pd content of 30%. For samples with 29% Pd, martensite transition occurs close to the triple point between fcc, ftc and bct phases, which leads to less softening presumably due to coherent irreversibly transformed bct nuclei.

Acknowledgments

The authors acknowledge financial support from the German DFG through SPP 1239, TP C4 (to IC and SGM), as well as the German Federal Ministry of Education and Research (BMBF) through PTJ-BIO, 0313909 (SGM), and thank K Samwer for the use of his splat quencher.

References

[1] Ullakko K *et al* 1996 *Appl. Phys. Lett.* **69** 1966
[2] Webster J, Ziebeck K R A, Town S L and Peak M S 1984 *Phil. Mag.* B **49** 295
[3] Mahnke G J, Seibt M and Mayr S G 2008 *Phys. Rev.* B **78** 012101
[4] Sozinov A, Likhachev A A, Lanska N and Ullakko K 2002 *Appl. Phys. Lett.* **80** 1746
[5] Cui J, Shield T W and James R D 2004 *Acta Mater.* **52** 35
[6] Kakeshita T and Fukuda T 2002 *Mater. Sci. Forum (Switzerland)* **394** 531
[7] James R D and Wuttig M 1998 *Phil. Mag.* A **77** 1273
[8] Ma Y, Zink M and Mayr S G 2010 *Appl. Phys. Lett.* **96** 213703
[9] Kühnemund L, Edler T, Kock I, Seibt M and Mayr S 2009 *New J. Phys.* **11** 113054
[10] Chmielus M, Zhang X X, Witherspoon C, Dunand D C and Mullner P 2009 *Nat. Mater.* **8** 863
[11] Kubota T, Okazaki T, Furuya Y and Watanabe T 2002 *J. Magn. Magn. Mater.* **239** 551
[12] Vokoun D, Hu C T and Kafka V 2003 *J. Magn. Magn. Mater.* **264** 169
[13] Nakajima H, Okazaki T, Kubota T, Sato M and Furuya Y 2004 *Mater. Trans.* **45** 2752
[14] Kishi Y, Yajima Z, Okazaki T, Furuya Y and Wuttig M 2008 *Adv. Sci. Technol.* **59** 24
[15] Kock I, Hamann S, Brunken H, Edler T, Mayr S G and Ludwig A 2010 *Intermetallics* **18** 877
[16] Edler T and Mayr S G 2010 *Adv. Mater.* **22** 4969
[17] Likhachev A A, Sozinov A and Ullakko K 2004 *Mater. Sci. Eng.* A **378** 513

[18] Kato H, Wada T, Liang Y, Tagawa T, Taya M and Mori T 2002 *Mater. Sci. Eng.* A **332** 134
[19] Liang Y, Wada T, Kato H, Tagawa T, Taya M and Mori T 2002 *Mater. Sci. Eng.* A **338** 89
[20] Hirth J P and Lothe J 1982 *Theory of Dislocations* (New York: Wiley)
[21] Duwez P, Willens R H and Klement W 1960 *J. Appl. Phys.* **31** 1136
[22] Nowick A S and Berry B S 1972 *Anelastic Relaxation in Crystalline Solids* (New York: Academic)
[23] Hohenberg P and Kohn W 1964 *Phys. Rev.* B **136** 864
[24] Blöchl P E 1994 *Phys. Rev.* B **50** 17953
[25] Kresse G and Joubert D 1999 *Phys. Rev.* B **59** 1758
[26] Perdew J P 1991 *Electronic Structure of Solids '91* ed P Ziesche and H Eschrig (Berlin: Akademie)
[27] Vosko S H, Wilk L and Nusair M 1980 *Can. J. Phys.* **58** 1200
[28] Kresse G and Furthmüller J 1996 *Phys. Rev.* B **54** 11169
[29] Gruner M E, Adeagbo W A, Zayak A T, Hucht A and Entel P 2010 *Phys. Rev.* B **81** 064109
[30] Zunger A, Wei S-H, Ferreira L G and Bernard J E 1990 *Phys. Rev. Lett.* **65** 353
[31] von Pezold J, Dick A, Friák M and Neugebauer J 2010 *Phys. Rev.* B **81** 094203
[32] Matsui M, Yamada H and Adachi K 1980 *J. Phys. Soc. Japan* **48** 2161
Matsui H and Adachi K 1989 *Physica* B **161** 53
[33] Bain E C 1924 *Trans. Am. Inst. Min. Metall. Pet. Eng.* **70** 25
[34] Opahle I, Koepernik K, Nitzsche U and Richter M 2009 *Appl. Phys. Lett.* **94** 072508
[35] Buschbeck J, Opahle I, Richter M, Rößler U K, Klaer P, Kallmayer M, Elmers H J, Jakob G, Schultz L and Fähler S 2009 *Phys. Rev. Lett.* **103** 216101
[36] Voigt W 1928 *Lehrbuch der Kristallphysik* (Leipzig: Teubner)
[37] Reuss A 1929 *Z. Angew. Math. Mech.* **9** 49
[38] Berryman J G 2005 *J. Mech. Phys. Solid* **53** 2141
[39] Kröner E 1958 *Z. Phys.* **151** 504
[40] Kakeshita T, Fukuda T, Terai T, Takeuchi T and Kishio K 2003 *J. Physique IV* **112** 93
[41] Granato A and Lücke K 1956 *J. Appl. Phys.* **27** 583
[42] Mullner P and Kriven W M 1997 *J. Mater. Res.* **12** 1771
[43] Glasstone S, Laidler K J and Eyring H 1941 *The Theory of Rate Processes* (New York: McGraw-Hill)
[44] Van Humbeeck J 1996 *J. Physique IV* **06** 371–80
[45] Finlayson T 1983 *Aust. J. Phys.* **36** 553
[46] Owen W S 1990 *Mater. Sci. Eng.* A **127** 197
[47] Edler T, Hamann S, Ludwig A and Mayr S G 2011 *Scr. Mater.* **64** 89
[48] Kock I 2010 *PhD thesis* Georg-August-Universität Göttingen http://webdoc.sub.gwdg.de/diss/2010/kock